Globular cluster formation within the Aquarius simulation

Article (Published Version)

Monthly Notices
of the
ROYAL ASTRONOMICAL SOCIETY

Mon. Not. R. Astron. Soc. **405,** 375–386 (2010) doi:10.1111/j.1365-2966.2010.16458.x

Globular cluster formation within the Aquarius simulation

B. F. Griffen,[1⋆] M. J. Drinkwater,[1] P. A. Thomas,[2] J. C. Helly[3] and K. A. Pimbblet[1,4]

[1]*Department of Physics, University of Queensland, QLD 4072, Australia*
[2]*Astronomy Centre, University of Sussex, Falmer, Brighton BN1 9QH*
[3]*Institute for Computational Cosmology, Department of Physics, University of Durham, South Road, Durham DH1 3LE*
[4]*School of Physics, Monash University, Clayton, Victoria 3800, Australia*

Accepted 2010 January 29. Received 2010 January 27; in original form 2009 September 25

ABSTRACT

The Aquarius project is a very high-resolution simulation capable of resolving the full mass range of potential globular cluster (GC) formation sites. With a particle mass $m_p = 1.4 \times 10^4$ M$_\odot$, Aquarius yields more than 100 million particles within the virial radius of the central halo which has a mass of 1.8×10^{12} M$_\odot$, similar to that of the Milky Way. With this particle mass, dark matter concentrations (haloes) that give rise to GCs via our formation criteria contain a minimum of ∼2000 particles.

Here, we use this simulation to test a model of metal-poor GC formation based on collapse physics. In our model, GCs form when the virial temperatures of haloes first exceed 10^4 K as this is when electronic transitions allow the gas to cool efficiently. We calculate the ionizing flux from the stars in these first clusters and stop the formation of new clusters when all the baryonic gas of the Galaxy is ionized. This is achieved by adopting reasonable values for the star formation efficiencies and escape fraction of ionizing photons which result in similar numbers and masses of clusters to those found in the Milky Way. The model is successful in that it predicts ages (peak age ∼13.3 Gyr) and a spatial distribution of metal-poor GCs which are consistent with the observed populations in the Milky Way. The model also predicts that less than 5 per cent of GCs within a radius of 100 kpc have a surviving dark matter halo, but the more distant clusters are all found in dark matter concentrations.

We then test a scenario of metal-rich cluster formation by examining mergers that trigger star formation within central gas discs. This results in younger (∼7–13.3 Gyr), more centrally located clusters (40 metal-rich GCs within 18 kpc from the centre of the host) which are consistent with the Galactic metal-rich population. We test an alternate model in which metal-rich GCs form in dwarf galaxies that become stripped as they merge with the main halo. This process is inconsistent with observed metal-rich globulars in the Milky Way because it predicts spatial distributions that are far too extended.

Key words: methods: numerical – stars: formation – Galaxy: formation – globular clusters: general.

1 INTRODUCTION

Globular clusters (GCs) provide a remarkably rich source of information about galaxy formation. Unlike the diffuse stellar populations of galaxies, GCs mostly contain stellar populations with a narrow range of ages and are extremely homogenous, making them relatively simple to understand and model. They are extremely old, so they survive as a record of conditions and processes of the earliest stages of galaxy formation (West et al. 2004). The properties of the Milky Way halo GC population led Searle & Zinn (1978) to conclude that the halo of our Galaxy formed via the slow accretion of many small protogalactic fragments, not via monolithic collapse as previously thought (Eggen, Lynden-Bell & Sandage 1962). In the 1990s, the (old) ages of GCs provided one of the motivations for considering cosmological models with non-zero cosmological constants (Ostriker & Steinhardt 1995).

In the last two decades, observations of extragalactic GC populations (notably with the *Hubble Space Telescope*) have revealed strong bimodality in the optical colours of GCs (e.g. Ashman & Zepf 1992). The blue population is identified as metal-poor clusters

⋆E-mail: griffen@physics.uq.edu.au

and very old, whereas the red population is more metal-rich and not as old.

These observations have motivated a number of competing galaxy and GC formation scenarios (e.g. Forbes, Brodie & Grillmair 1997; West et al. 2004), which attempt to explain the bimodal colours, but no conclusive theory has emerged. However, the very existence of the bimodal colours is indicative of two epochs of star formation. In view of the large amount of data collected, there is a strong need for more detailed theoretical work that will provide specific predictions of where and when GCs formed (Ashman & Zepf 1998; Brodie & Strader 2006).

In contrast with the extensive gains from observational studies of GCs, it has proven very difficult to predict the full range of observed GC properties in a self-consistent manner from theoretical models. The mass and spatial scales needed to study the physical conditions of GC formation are very difficult to simulate numerically in large models.

The problem of direct simulation was avoided in an early study by Beasley et al. (2002), who used a semi-analytic model of galaxy formation in a cold dark matter universe. They assumed that GCs would form in each galaxy in numbers proportional to the numbers of stars forming (given by the semi-analytic model). They could then ascribe chemical properties to the GCs according to the same model. Their model successfully reproduces bimodal GC populations and other observations, but only if they invoke a truncation of metal-poor GC formation at redshift $z > 5$. This truncation was also investigated by Bekki (2005) in a collisionless dark matter simulation of the formation of a single galaxy (mass resolution of $4 \times 10^7\,\mathrm{M}_\odot$) with the simplifying assumption that GCs formed in all low-mass subhaloes forming before some truncation redshift. Bekki shows that the final ($z = 1$) radial distribution of the objects is very sensitive to the truncation redshift which was set at $z \approx 15$ to match the GC distribution of the Milky Way. In a more general study of structure formation Moore et al. (2006) identified reionization as the process responsible for the truncation, assuming that it took place by $z \approx 12$. They went on to suggest that the radial distribution of GCs and satellite galaxies could be used to constrain models of the reionization process. These last two studies established the importance of reionization and the truncation of GC formation, but were not able to calculate the important parameters directly.

A more comprehensive approach to the problem was taken by Kravstov & Gnedin (2005) who combined both gas and *N*-body codes to model a Milky Way sized galaxy, although the simulation only ran to a redshift of $z = 3$. Their model used the assumption that GCs formed in sufficiently massive giant molecular clouds – themselves in the discs of protogalaxies. This work was successful in matching several observed GC properties such as masses and sizes, but could not predict present-day positions. It was – like the earlier work – very reliant on assumptions about the conditions necessary for GC formation.

The *N*-body (dark matter) and semi-analytic approaches have recently been combined in a large-scale cosmological simulation by Bekki et al. (2008) to model the dynamical and chemical properties of GCs in a wide range of galaxies. The simulation covers a large volume, so the mass resolution is relatively low ($\sim 3 \times 10^8\,\mathrm{M}_\odot$) compared to GC masses; they simulate GC formation by assuming that every virialized dark matter halo of 10 or more particles will form a GC. They also rely on a truncation of metal-poor GC formation due to reionization at $z_{\mathrm{trunc}} = 6$ (this value being based on quasar data; see the discussion below). From their model, Bekki et al. (2008) obtain old ages for both metal-rich GCs (peaking at $z \sim 4$) and metal-poor GCs (peaking at $z \sim 6.5$) and also obtain bimodal metallicity distributions for about half the galaxies. They also find that the galaxies without bimodal distributions tend to be small galaxies which lack metal-rich GCs. The model also produces more centrally concentrated distributions for the metal-rich GCs than for the metal-poor GCs, although the physical origin of this difference is not specifically discussed.

A common feature of the simulations described above is the reliance on ad hoc assumptions to identify the sites where GCs form. This was inevitable because the mass resolution was too low to resolve individual GCs. In this paper, we present the first study of GC formation based on a simulation in which GC masses are well resolved.

We use the Aquarius suite of simulations (Springel et al. 2008, hereafter S08), the highest resolution simulations of Milky Way sized haloes done to date. It must be emphasized that this is the first work in which each GC formation site is *directly* resolved with a *minimum* of about 2000 particles. Although this first paper is based strictly on the dark matter components of the simulation, the exquisite resolution allows us to calculate the conditions for metal-poor GC formation directly. We also include a more qualitative model for the formation of metal-rich GCs which successfully predicts their centrally concentrated distributions.

Our model for metal-poor GC formation is different from previous work in two major aspects. First, we model the formation by directly identifying when and where the early haloes first reach a temperature of 10^4 K, the threshold temperature above which rapid cooling takes place leading to collapse and star formation. Secondly, we do not assume an arbitrary value for the redshift when GC formation is truncated. Instead, we directly estimate the number of ionizing photons emitted by these early clusters and stop their formation when there are enough photons to ionize the entire galaxy.

We have used the simulation to test two models for the formation of the metal-rich GC population: (i) the stripping of GCs from disrupted satellite galaxies and (ii) the formation of star clusters in the gas disc of the forming galaxy, triggered by large merging events. We find that only the second model can produce the centralized distribution of metal-rich GCs as observed in the Milky Way.

The structure of this paper is as follows. In Section 2, we describe the Aquarius suite of cosmological simulations and our models for forming GCs in the simulations. In Sections 3 and 4, we present the results of our models in detail, notably comparing the spatial distributions with observations, first for the metal-poor GCs and then for the metal-rich GCs. We then discuss our results in Section 5 and conclude by summarizing our results and future work in Section 6.

2 MODELS OF GLOBULAR CLUSTER FORMATION

In this section, we describe the methodology of our study: how we identify the GC formation sites in the Aquarius simulation data. We start by summarizing the relevant details of the simulations themselves. We then describe our models for metal-poor and metal-rich GC formation in detail in Sections 2.2 and 2.3, respectively.

2.1 The Aquarius simulations

The Aquarius Project actually consists of simulations of six different Milky Way sized galaxies, one of which is analysed in this paper. Although a detailed description of the simulations can be found in S08, we review the pertinent details here.

Table 1. The basic parameters of the Aquarius simulation data used in this paper.

Name	m_p ($M_\odot$)	ϵ (pc)	N_{hr}	N_{lr}	M_{200} ($M_\odot$)	r_{200} (kpc)	M_{50} ($M_\odot$)	r_{50} (kpc)	N_{50}
AqA2	1.370×10^4	65.8	531 570 000	75 296 170	1.842×10^{12}	245.88	2.524×10^{12}	433.52	184 243 536
AqA3	4.911×10^4	120.5	148 285 000	20 035 279	1.836×10^{12}	245.64	2.524×10^{12}	433.50	51 391 468

Note. m_p is the particle mass, ϵ is the Plummer equivalent gravitational softening length, N_{hr} is the number of high-resolution particles and N_{lr} the number of low-resolution particles filling the rest of the volume. M_{200} is the virial mass of the halo, defined as the mass enclosed in a sphere with mean density 200 times the critical value. r_{200} gives the corresponding virial radius. We also give the mass and radius for a sphere of overdensity 50 times the critical density, denoted as M_{50} and r_{50}. Note that this radius encloses a mean density 200 times the background density. Finally, N_{50} gives the number of simulation particles within r_{50}.

The starting cosmological parameters for Aquarius are the same as used in the Millennium Simulation (Springel et al. 2005). Halo formation is tracked within a periodic box of side $100\,h^{-1}$ Mpc in a cosmology with parameters $\Omega_m = 0.25$, $\Omega_\Lambda = 0.75$, $\sigma_8 = 0.9$, $n_s = 1$, and Hubble constant $H_0 = 100\,h\,\mathrm{km\,s^{-1}\,Mpc^{-1}} = 73\,\mathrm{km\,s^{-1}\,Mpc^{-1}}$. We use a baryon fraction $\Omega_b/\Omega_m = 0.18$ to convert from dark matter mass to baryonic mass. It must be clearly stated that the simulations used for this work utilized only the dark matter components and did not include baryons.

Millennium Simulation haloes of roughly Milky Way mass and without close neighbours at $z = 0$ were selected for resimulation using 900^3 particles in a box of dimension $10\,h^{-1}$ Mpc. Identifying the Lagrangian region from where each halo formed, the mass distribution was rerun at a much higher spatial and mass resolution. Distant regions were sampled with more massive particles, but retained sufficient resolution to ensure an accurate representation of the tidal field at all times. For greater detail on the simulation, see S08.

A major feature of the simulations is the identification of substructure – the bound mass concentrations that will grow and merge over time to build structure. These are identified and measured in Aquarius using the same SUBFIND (Springel et al. 2001) algorithm used for the Millennium Simulation. Although SUBFIND outputs are commonly called 'subhaloes', we use the words subhalo and halo interchangeably to represent potential GC structures. This is because a potential GC can be classed as either an object within a much larger parent object (i.e. a subhalo) or an object outside the virial radius of any other halo (i.e. a halo). For future reference, wherever we state the words 'halo' and 'subhalo', we are referring to the same thing, the SUBFIND outputs.

The way in which the haloes are linked between time-steps works as follows. For each halo, we take the most bound 10 per cent of its particles and determine which halo they belong to at the next snapshot. The halo at the later time with the largest number of these particles is identified as the descendant. In most cases, this is all that is required. However, there are occasional cases where SUBFIND fails to identify a halo at one or more snapshots but picks it up again at a later time. For example, this can happen if a halo passes close to the centre of a larger halo. We attempt to deal with this by looking for descendants more than one snapshot later if a halo is not the most massive progenitor of the descendant identified using the procedure described above or if no descendant is identified. A halo which exists up to three snapshots later will be identified as the descendant if it contains more than half of the 10 per cent most bound particles from the original halo and has no identified progenitors.

All these different data structures between time-steps for each simulation are stored in a data base very similar to that of the Millennium project.[1] We also make use of the raw particle data in the cases where we are unable to obtain the SUBFIND halo information to track material from haloes that have merged. This is discussed in further detail in Section 2.2.2.

Each of the six Aquarius haloes was calculated using at least two different particle masses ('resolutions') to test for convergence. We selected our highest resolution halo ('A' halo) for our GC study in this paper and analysed it at two different resolutions so as to check our results for any dependence on simulation resolution. A summary of the two data sets is given in Table 1.

2.2 Formation of metal-poor GCs

2.2.1 Temperature threshold

We use a relatively simple model to identify where the metal-poor GC-type objects would form within the Aquarius simulation based on the conditions necessary for the collapse of a proto-GC gas cloud and subsequent star formation. All the recent simulations rely on a similar model for GC formation (dating back to Peebles 1984), but the resolution of Aquarius allows us to measure the main parameter – temperature – directly.

The gas clouds cannot collapse without an efficient cooling mechanism: in the absence of a significant number of heavy elements, the main cooling processes are the collisional excitation of hydrogen and helium, radiative recombination of hydrogen and bremsstrahlung (e.g. Nishi 2002). The typical cooling function for primordial gas in the equilibrium state reveals an extremely rapid increase in the cooling rate as the temperature increases to 10^4 K. We therefore adopt 10^4 K as a temperature threshold, above which gas clouds can efficiently cool and collapse to form GCs.

Given the very large mass of gas required to form a GC (see Section 3.1), the early protocluster gas clouds must form in the potential wells of the dark matter subhaloes identified by SUBFIND. By assuming that the gas is in quasi-static equilibrium with the dark matter, we can use the virial theorem to relate the 1D internal velocity dispersion measured of the dark matter subhaloes (σ_v) to the (inferred) virial temperature of the gas, T_v:

$$\sigma_v^2 = \frac{kT_v}{\mu m_H}, \quad (1)$$

where m_H is the mass of a hydrogen atom and μ is the mean molecular weight of the gas. We adopt a molecular weight of $\mu = 0.58$, appropriate for a fully ionized, primordial gas. Our 10^4 K temperature threshold therefore corresponds to a 1D velocity dispersion of $\sim$11.9 km s^{-1}.

[1] http://www.g-vo.org/Millennium

We identify metal-poor GC formation sites by searching the entire merger tree of the simulation for any subhaloes that exceed the 10^4 K threshold for the first time.

2.2.2 *The final positions of disrupted subhaloes*

Although we have excellent resolution to directly locate where candidates first form, it is no longer possible to locate these structures as distinct subhaloes at redshift zero if they have undergone merging events with either each other or the central host halo since it leads to their complete destruction. We address this problem by using the most bound particle of each subhalo as a marker to track its final position. This is equivalent to assuming that the collapsed baryonic gas forming a GC at the centre of each subhalo will follow a similar trajectory to the most bound particle. We simply search the final simulation snapshot at $z = 0$ to locate where each of these uniquely identified particles resides. This directly allows us to follow GC formation sites through to the present day.

As we show below, the majority of the haloes containing GC formation sites merge with the central halo by the present day, but some survive in separate haloes at a range of distances. We include both groups in our model (both merged and surviving haloes) but we restrict our discussion to the GC candidates that end up being associated[2] with the main Milky Way halo in the simulation at redshift zero. There are a few objects in the outer halo that do not satisfy this condition; we discuss these further in Section 5.

2.2.3 *Reionization within Aquarius from the first GCs*

Previous simulations of GC formation have found it necessary to truncate the formation process after a certain redshift in order to avoid producing unrealistically large numbers of clusters (Bekki 2005; Kravstov & Gnedin 2005; Bekki et al. 2008). The truncation redshift has generally been set on the basis of external estimates of the redshift of reionization. In this paper we take a different approach, based on an internal calculation of the ionization from the first star clusters themselves.

The possible sources of reionization discussed in the literature include active galactic nuclei, Population III massive stars and binaries. By varying two free parameters (minimum quasar luminosity and star formation efficiency), Srbinovsky & Wyithe (2006) found that the relative contribution made by quasars to the ionizing background at $z = 5.7$ is between 1.4 and 14.5 per cent. The key parameter of measuring quasar contributions observationally (from the quasar spectra) is the escape fraction of Lyα photons from galaxies into the intergalactic medium (IGM), $f_{\rm esc}$. Unfortunately, this approach cannot yet be applied; there is a wide range of estimates of $f_{\rm esc}$ (Madau & Shull 1996; Bianchi, Cristiani & Kim 2001; Ricotti 2002) and at best they are upper limits, as the absorption of ionizing radiation from the molecular cloud and dust extinction are ignored. This uncertainty, coupled with the relative scarcity of quasars at redshifts greater than $z \sim 4$, points to another source of ionization. However, in terms of determining when the redshift of reionization ended, observations of Lyα systems in high-redshift quasars indicate that the IGM was fully ionized at $z \sim 6$ (Gnedin & Hamilton 2002).

[2] By associated, we mean fully merged either with the main halo or in surviving haloes that are within two times the half-mass radius ($2\,r_{1/2} = 150$ kpc) of the main halo at redshift zero.

Sokasian et al. (2004) coupled a radiative transfer calculation with a high-resolution hydrodynamical simulation to study the contributions from high-z stellar sources and found that Population III stars can account for as much as 66 per cent of the mean level of ionization reached by $z = 16$ if the escape fraction of photons is of order unity and there is no limit on the number of stars that can form within a given halo. Power et al. (2009) investigated the contributions of X-ray binaries within GCs and found that, depending on the survival fraction, a single GC of 10^6 stars can ionize $5 \times 10^7\,{\rm M}_\odot$ of neutral hydrogen during its first 100 Myr. Our own calculations (below) show that the stars in the GCs themselves contribute at least as much to the total level of reionization. Given the uncertainties in each process we base our reionization calculation on the GC contribution, noting that this is effectively scaled to include the contributions from other sources.

In this work, we estimate the ionizing contribution of massive stars within the forming galaxy directly from the simulation. We assume that the local ionizing radiation is dominated by flux from the first GCs to form. We calculate the number of ionizing photons from each GC using a Salpeter initial mass function (IMF) based on Population II star formation models from the STARBURST99 code by Leitherer et al. (1999). We do not aim to ionize the entire IGM; instead, we specifically ask if local ionizing photons from the first GCs are sufficient to ionize the *intra*-galactic medium of the forming galaxy by some redshift, $z_{\rm ion}$. Our full calculation in Section 3.1 shows that this does happen and at earlier redshifts than given by the quasar estimates.

2.3 Formation of metal-rich GCs

It is more difficult to model the formation of the metal-rich GC population in our simulation. First, the defining chemical makeup of this population can only be modelled if we include baryonic gas processes. Secondly, although these clusters are slightly younger than the metal-poor GCs, they are actually the more centrally concentrated of the two populations in the Milky Way. This is counter to what happens in hierarchical merging processes where the first objects to form end up being the most centrally concentrated. We have considered two very simple models that can be tested qualitatively with our current simulation data.

2.3.1 *Model 1: tidal stripping of satellite dwarf galaxies*

Based on previous models of tidal interactions removing the outer envelopes of dwarf elliptical (dE) galaxies (Bekki 2005), we investigated a stripping model of GC formation. The basic idea here is that the dwarf galaxies have formed their own (metal-rich) GCs that survive to join the main halo after the dwarf is disrupted. We tested this model by identifying as 'stripped' any halo which merges with a more massive halo (typically, the mass increase in such a merger is a factor of 10 or more). The maximum mass of the progenitor halo, before merging, is taken to be proportional to the mass of the nuclear GC that forms within it.

As we show in Section 4, this results in far too extended a distribution. This is the problem mentioned earlier that, in hierarchical models, younger objects have less centrally concentrated distributions than older ones.

2.3.2 *Model 2: major mergers with the central halo*

The proposal that metal-rich GCs are formed in gas-rich mergers of interacting galaxies has been around for quite some time. Toomre

& Toomre (1972) were the first to investigate these merger events in detail but it was not until much later that the formation of GCs in this framework was discussed (Schweizer 1987). *Hubble Space Telescope* observations of young massive star clusters forming in the merging Antennae galaxies (Whitmore & Schweizer 1995) provided strong motivation for this model (see also Holtzman et al. 1992) which remains the subject of many studies (Zepf 2009). Although some of the observations of star-forming regions are situated within a massive merger which may go on to become an elliptical, one could argue that because the bulges of spirals form through mergers in much the same way as ellipticals, the GCs will form in the bulges of spirals in much the same way as they form in ellipticals. A caveat of this work is that secular evolution and bars may also contribute to bulge formation which will have an appreciable effect on the build-up of the Milky Way itself but not necessarily on its GC population.

We adopt the following simple model of metal-rich GC formation by gas-rich mergers. We search the merger tree for any halo (above some mass threshold) which merges with the central halo. We adopt the premise that during the merger event, stars will form via perturbations in and around the gas disc of the central halo at that particular redshift. Since the merging haloes are destroyed in this process, the location (radius with respect to the central halo) of where the stars form can be approximated by the radius of the gas disc. This we assume is a fraction of the half-mass radius of the central halo at the redshift of the merger event. Since we have access to the half-mass radius of the central halo at each time-step, we essentially count the number of merger events at a given time-step and say that all of those infalling haloes will create stars at some fixed fraction of the half-mass radius.

We adopt the major-merger scenario here because it is motivated not only by a range of observational results, but it is also the only model we can find which can make metal-rich GCs with a more concentrated distribution than the metal-poor GCs, as is observed in the Milky Way. Although our motivation mainly comes from observations of major mergers which will eventually turn the GC host into an elliptical, we suppose that the merging process induces star formation during a merger event independent of what the resulting host structure will be. The overall assumption in our models is that metal-poor GCs as the first primordial objects which were later truncated and metal-rich GCs were formed in merger events during later epochs of hierarchical build-up.

2.4 Distinction between GC models

In summary, the difference between the two models is as follows: metal-poor GCs are those dark matter concentrations which first exceed the temperature threshold (10^4 K, discussed in Section 2.2) during the simulation. Their ionization contributions are measured and when the ionized mass reaches the mass of the entire galaxy, we no longer form any more GCs. The metal-rich GCs, however, are identified in an entirely different manner. We trace the merger tree of all haloes and define our sample as haloes which (i) have undergone a significant merger event with the host and (ii) have been above a particular mass threshold prior to the merger event.

3 METAL-POOR GLOBULAR CLUSTERS

We identify candidate haloes for metal-poor GCs using the method described in Section 2.2. The redshift distribution of the haloes is shown in Fig. 1.

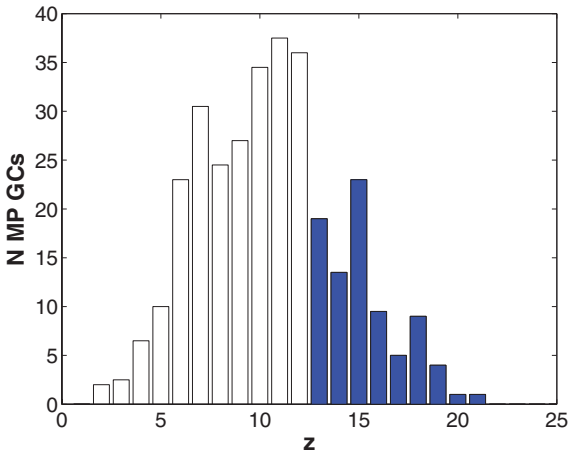

Figure 1. Formation history of all metal-poor (MP) GCs. The figure shows the redshift when they first exceed a virial temperature of 10^4 K. The filled bars represent those haloes that form before $z_{\rm ion}$ ($z_{\rm ion} = 13, t_{\rm look-back} = 13.6$ Gyr). The hollow bars are the remaining haloes identified above the temperature threshold but are suppressed due to the ionizing contributions (see Section 3.1) from the (blue) haloes that formed earlier. By $z = 13$, the entire Galaxy has been ionized.

There are two things to note about this distribution. First, there are far too many GC candidates for a Milky Way sized galaxy, and secondly the distribution extends down to low redshift. We address these concerns by estimating, in the following section, the redshift at which the GCs that form can reionize the protogalaxy. Those haloes that form after reionization are shown as hollow bars in the figure.

3.1 Reionization contributions

We define an ionizing efficiency, $F_{\rm ion}$, to determine the mass of gas ionized by each GC in our model. $F_{\rm ion}$ is the mass of baryons ionized by the GC divided by the baryonic mass of the halo in which the GC first forms (assuming that each of our GC formation sites forms only one GC). Each GC can therefore ionize a region greater in baryonic mass than itself by a factor of

$$F_{\rm ion} = f_{\rm sfe}\, \bar{q}\, f_{\rm esc}, \qquad (2)$$

where $f_{\rm sfe}$ is the star formation efficiency (the fraction of the protocluster baryonic mass that forms stars), $\bar{q}$ is the mean number of ionizing photons per baryon locked up in stars and $f_{\rm esc}$ is the fraction of those photons that escape the cluster. In writing down this expression, we assume that one ionizing photon per baryon is sufficient to ionize the surrounding gas out to $2r_{1/2}$ (where $r_{1/2} = 75$ kpc is the dark matter half-mass radius of the main halo in both simulations). This radius contains the majority of the GCs and of the baryonic mass of the galaxy. This is a reasonable approximation given the uncertainties in the other factors.

For a self-gravitating gas cloud, star formation efficiencies of the order of one-third or more are required in order to form a bound cluster (Baumgardt & Kroupa 2007). However, if not all the gas in a halo ends up in the protocluster the star formation efficiency could be considerably lower. Here we take $f_{\rm sfe} = 0.07$ because this gives masses for the GCs that seem to agree with observations – see Section 3.2.

The number of ionizing photons emitted per baryon of stellar material depends strongly upon the stellar mass. We use the

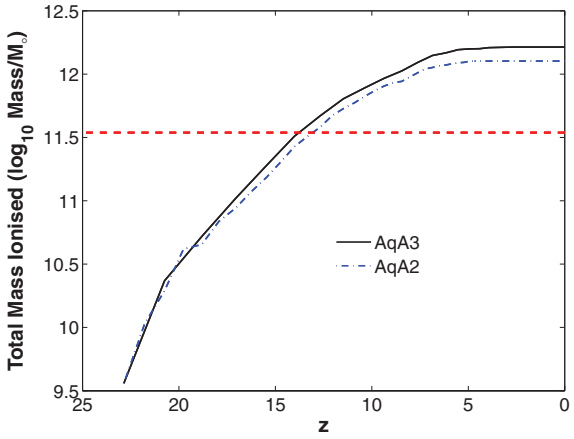

Figure 2. Cumulative mass of baryons ionized by metal-poor GCs for both high (black, solid line) and low (blue, dot–dashed line) resolution runs. The total baryonic mass of the central galaxy at the present day is given by the red-dashed line.

Population II efficiency curve of fig. 2 from Tumlinson, Venkatesan & Shull (2004) (calculated using the STARBURST99 code of Leitherer et al. 1999). Averaging over a Salpeter IMF (see Appendix A) gives $\bar{q} \approx 10\,000$. This figure could be raised by moving towards a more top-heavy IMF. Note that the lifetime of a $10\,M_\odot$ star is around 40 Myr, of the order of the dynamical time of the first GC haloes that form and less than the dynamical time in later ones. It is a reasonable approximation therefore to assume instantaneous feedback.

As discussed in Section 2.2.3, the escape fraction of photons is the most uncertain factor. To obtain the correct number density of metal-poor GCs, we require $f_{\rm esc} = 0.3$, which is not unreasonable given the escape fraction in the early Universe would be considerably higher than we observe locally.

Putting all these factors together, we have $F_{\rm ion} \approx 210$. Fig. 2 shows the cumulative mass of ionized gas for the AqA2 halo, starting at high redshift and moving towards the present. Note that we only include the contribution from GCs that end up within $2r_{\rm half} = 150$ kpc of the central halo in the present day. The two curves correspond to the two different numerical resolutions and show good agreement – at $z = 13$ the difference between the two curves represents less than one output time in the merger tree construction. The dashed line shows the total baryonic mass of the halo at the present day (i.e. the mass within a sphere centred on the most bound particle and enclosing a mean density of 200 relative to the critical density).

The radiation produced by the metal-poor GCs is sufficient to ionize a mass equal to that of the present-day galaxy by a redshift of about 13 (Fig. 2). There is a lot of uncertainty in this estimate and varying $F_{\rm ion}$ by a factor of 2 could give an estimated ionization redshift in the range 10–15. However, using $F_{\rm ion} = 210$ ($z = 13$) gives a number of clusters that agree well with observations and so we stick with that for the rest of our analysis.

Using this value for the reionization cut in AqA2, we define a total sample of 173 metal-poor GCs, of which 125 lie within the $2r_{1/2}$ of the central halo. The majority of these (105) are no longer in separate dark matter haloes, but have merged with the central halo. The number of GCs we form is quite consistent with the number of metal-poor GCs observed in the Milky Way (103 with [Fe/H] < -1; Harris 1996).

3.2 Masses

In order to calculate the present-day masses of our metal-poor GCs, we first need to know what fraction of the baryonic mass of a gaseous protocluster becomes locked up in stars. Baumgardt & Kroupa (2007) and Weidner et al. (2007) found that in order to form a bound star cluster, a protocluster requires a star formation efficiency of approximately 0.3. However, this can be much lower if not all the gas within the halo cools to become part of the protocluster; for example, the cluster may form from a small fraction of the gas that has condensed at the centre of the halo. In this paper, we adopt a value of 0.07 as this gives present-day GC masses that seem to agree with those in the Milky Way.

We then require an estimate of how much mass loss due to stellar evolution (winds, supernovae) and dynamical evolution from tidal stripping and evaporation affects the cluster. Kruijssen (2008) showed that a typical GC loses ∼70 per cent of its initial stellar mass and this is the value that we adopt here. Overall, this means that we have from an initial dark matter mass of $M_{\rm DM,0}$ a final present-day stellar mass of $0.18 \times 0.07 \times 0.3 M_{\rm DM,0} = 0.0038 M_{\rm DM,0}$.

Fig. 3 compares both our candidates identified before $z = 13$ to those of the Milky Way with [Fe/H] < -1 [assuming $M/L_v = 3$ for 13 Gyr old stellar population (Maraston 2005)]. We obtain a range of masses between $\sim 10^5$ and $10^6\,M_\odot$ (rms $= 2.8 \times 10^5\,M_\odot$). The masses are consistent with the mean of, but have a narrower spread than, the observed Milky Way GCs' mass distribution. This may be due to observational errors in calculating the mass and/or scatter in the mass loss from individual clusters. It must be restated that the haloes are well resolved. The lowest mass object in Fig. 3 is an *inferred* stellar mass. The actual dark matter mass of our smallest $10^5\,M_\odot$ baryonic GC is $\sim 10^7\,M_\odot$. This will contain ∼2000 particles.

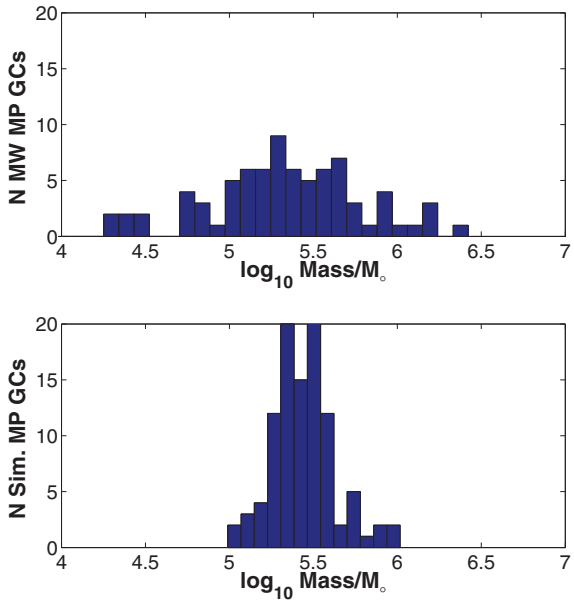

Figure 3. Comparison of the masses of simulated metal-poor (MP) GCs with the observed masses of Galactic GCs. Top panel: number of Milky Way GCs with a given mass for those with available integrated V-band luminosities [calculated from the Harris (1996) catalogue assuming $M/Lv = 3$ and including only metal-poor GCs with [Fe/H] < -1]. Bottom panel: calculated present-day masses of our GC candidates (AqA2 resolution) that formed before $z = 13$.

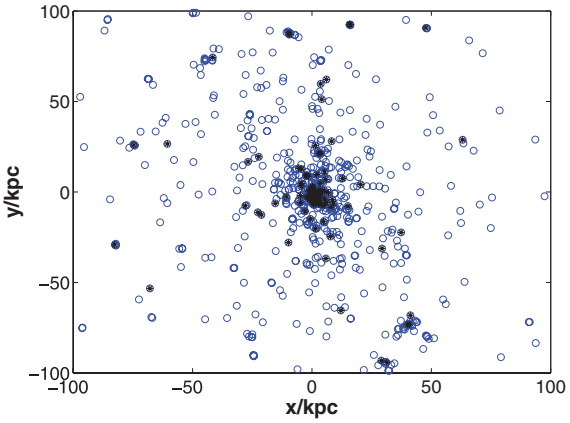

Figure 4. Present-day spatial x–y distribution demonstrating the effect of including (filled circles) and excluding (open circles) metal-poor GC truncation at $z_{\rm trunc} = 13$ for the AqA2 halo. Without including reionization, there are far too many GCs, particularly at large radii.

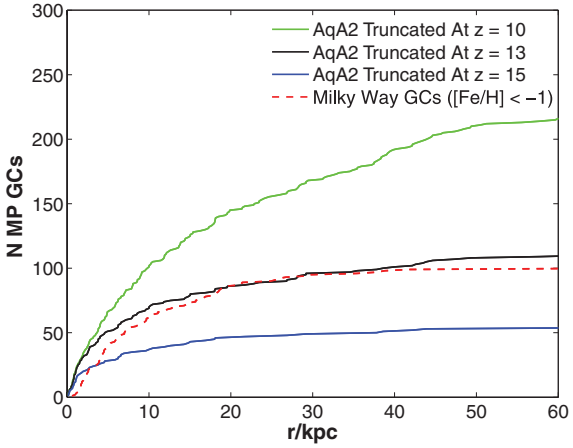

Figure 5. Spatial distribution of both model and observed metal-poor GCs. The curves show the cumulative radial distributions of each population. Three different model populations are shown, corresponding to the three ionization cuts discussed in the text (solid lines). The dashed line shows the observed distribution of metal-poor GCs in the Milky Way (Harris 1996).

3.3 Ages

With the reionization cut, all the metal-poor GCs form in the redshift range 22–13, corresponding to look-back times of 13.3–13.5 Gyr. The precise age of the GCs presumably mimics the assembly time of the galactic halo, but the prediction of a narrow spread in ages will hold for all galaxies.

This is broadly consistent with the observations of the Milky Way. From age dating of Galactic GCs from the Advanced Camera for Surveys (ACS) survey carried out by Marín-Franch et al. (2009), we know that the majority of the metal-poor GCs ([Fe/H] < -1) formed approximately 13 ± 1.5 Gyr ago with a narrow spread in ages, consistent within the errors with a single formation redshift.

3.4 Spatial distribution

Fig. 4 shows a projection of the final GC locations relative to the most bound particle in the host galaxy. Filled circles represent those clusters that form before our reionization cut and open circles those that form afterwards. The latter population is much more extended than the former; this is to be expected as they form later.

Fig. 5 shows a present-day cumulative radial distribution of the Milky Way metal-poor GCs and the AqA2 metal-poor GCs using three different reionization cuts, corresponding to $F_{\rm ion} = 105$, 210 and 420. The radial distributions of the Milky Way GCs and of our model GCs are in agreement, whereas earlier forming haloes are too centrally concentrated and later forming ones too extended. This is very strong evidence that the metal-poor GCs do indeed form in the high-redshift haloes that we have identified. A Kolmogorov–Smirnov (KS) test carried out comparing the three distributions against the Milky Way GCs found that we could reject only the $z = 10$ model (at $P < 0.01$). Although we know that it should not produce the Milky Way distribution, formally we show that under the KS test two of the populations have distributions consistent with the Milky Way observations.

3.5 Kinematics

The limited observational evidence on the kinematics of metal-poor GC populations in late-type galaxies is described in Brodie & Strader (2006). There is some indication that different sub-

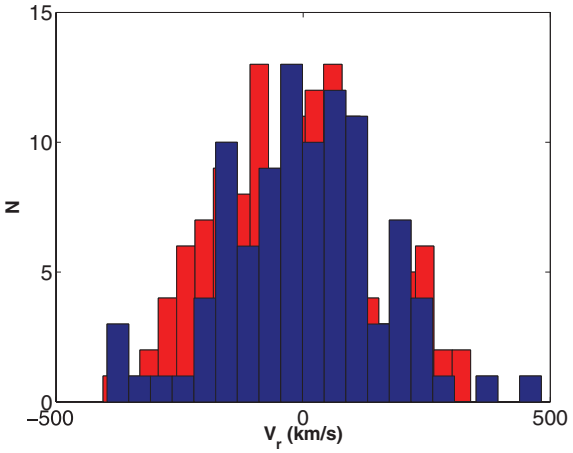

Figure 6. Heliocentric radial velocities of both observed (blue) (Harris 1996) and AqA2 (red) GCs.

populations may have different rotation properties, as if the galaxies have been built up from mergers of smaller systems. This is consistent with the idea that metal-poor GCs formed early on, before their host galaxy.

Overall, there appears to be little net rotation of the observed metal-poor GC population. Our models agree with this result, showing rotation speeds of the order of 10 km s^{-1} that are consistent with no net rotation within the sampling errors.

The velocity dispersion of the model GC population is radially biased, having an anisotropy parameter of $\beta = (3/2)\,(1 - \sigma^2/\sigma_{\rm r}^2) \approx 0.6$ (here $\sigma_{\rm r}$ and σ are the rms radial and total velocities relative to the Galactic Centre, respectively). Fig. 6 shows the heliocentric radial velocities of both the observed Milky Way and Aquarius GC populations. They are not inconsistent with each other. The observational evidence is currently too weak to place strong constraints on β.

4 METAL-RICH GLOBULAR CLUSTERS

The Milky Way metal-rich GC population is more centrally concentrated than is the metal-poor one. This is a problem for any

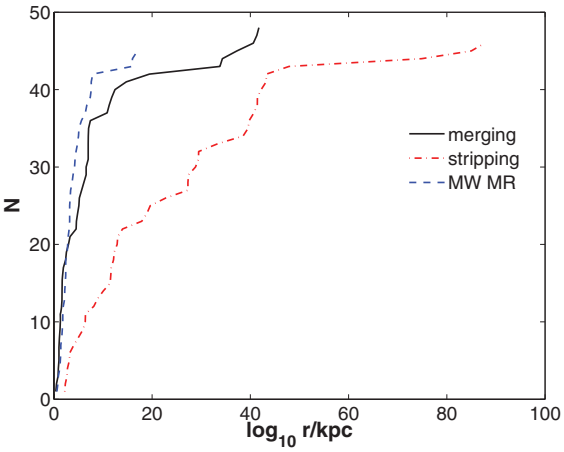

Figure 7. The radial distribution of metal-rich (MR) GC candidates from the stripping model (dot–dashed line) and the merging model (solid line) compared to their distribution in the Milky Way (dashed line).

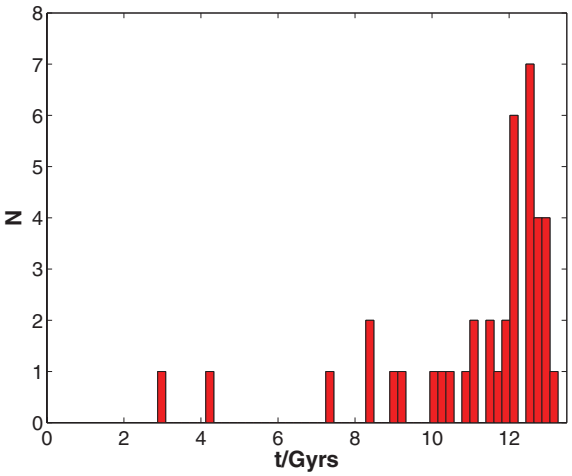

Figure 8. The distribution of ages for metal-rich GCs formed using the merger model.

formation model that invokes accretion from haloes more massive, and hence later forming than those used to define the metal-poor population. As an example, we show in Fig. 7 the present-day distribution of metal-rich GCs in a model in which they are the nuclei of stripped dwarf galaxies that have been disrupted by the tidal forces of the Galaxy. In this plot, we estimate the current location of the GC from that of the most bound particle in the dwarf galaxy at the time-step before it lost its identity. In order to match the observed number of metal-rich GCs in the Milky Way, we have included dwarf galaxy haloes whose maximum mass before disruption exceeded 8×10^8 M$_\odot$ but other mass cuts produce similar profiles. As can be seen from the plot, the radial distribution of such objects is far too extended and cannot possibly represent the metal-rich GC population.

To find a distribution that is more centrally concentrated than that of the metal-poor GCs, we must abandon models that form clusters within subhaloes and instead form them directly within the galaxy itself. As mentioned in Section 2.3.2, there is observational evidence for the formation of massive star clusters in merging galaxies and so this is the model that we turn to here.

It is not obvious how large a merger is needed in order to generate enough disturbance to trigger GC formation. To match the number of metal-rich GCs in the Milky Way, we assume that a single GC forms whenever a galactic halo of mass 8×10^8 M$_\odot$ or more merges with a larger halo. We further need to assume that the infalling halo must have a mass of at least 1 per cent of the mass of the larger one; otherwise large numbers of GCs would be formed by accretion of small satellites on to the galaxy at late times.

The GCs will form at the centre of the halos as that is where the cold gas is located. For satellite haloes, we use the location of the most bound particle as a tracer of the GC position at later times. For the main halo, we assume that the GC forms at a small fraction, 0.1, times the half-mass radius.

There are a lot of ad hoc assumptions in this model: we do not know how massive an infalling satellite must be to trigger GC production, we do not know how many star clusters will form and what their mass will be and we do not know the precise location in which they will form. Nevertheless, we present broad-brush results below in order to demonstrate that the model GCs have approximately the right properties and to motivate further study.

4.1 Spatial distribution

The present-day spatial distribution of the GCs formed in the merging model is shown as the dashed line in Fig. 7. The central concentration of GCs within 15 kpc originates from mergers with the main halo. This agrees well with the observed distribution of metal-rich GCs in the Milky Way. In addition, about a quarter of the GCs result from mergers in satellite galaxies that later fell into the main halo. These latter objects have a more extended distribution and do not seem to have analogues in the Milky Way metal-rich GC population. The most important feature of Fig. 7 is not necessarily that we obtain the correct number by a given radius, but how centralized the distribution is compared to the Milky Way. Although the merging model may not overlap the Milky Way population, it is the best of our models that produces the required concentrated distribution.

4.2 Ages

In Fig. 8, we show the number of metal-rich GCs formed as a function of look-back time. Also shown, for comparison, are the metal-poor GCs.

We know from various observational studies of metal-rich GCs that the majority formed over a much larger temporal range than metal-poor GCs, probably because they form via processes which require larger dynamical times (Harris 1996; Salaris & Weiss 2002; De Angeli et al. 2005; Marín-Franch et al. 2009). These observations are broadly consistent with our findings. However, there are two GCs that have younger ages, between 3 and 4.1 Gyr, which are shown in the far left of Fig. 8. It is possible that they are an accident of the formation history of this particular galactic halo or that the galactic disc has become so depleted by these late times that it is no longer susceptible to GC production in minor mergers.

5 DISCUSSION

In this section, we discuss more general aspects of our simulation of the GCs starting with the achievements and limitations of the models.

The model proposed in this paper for the formation of metal-poor GCs is based on just two parameters: the temperature threshold for cooling and the ionizing efficiency, $F_{\rm ion}$. The first of these is fixed by cooling physics and is not a variable in the model. The

second parameter, the ionizing efficiency, is actually a product of three relatively uncertain factors: the star formation efficiency, the number of ionizing photons and (especially) the escape fraction of photons as discussed in Section 3.1. In our calculation of $F_{\rm ion}$ we have chosen reasonable values for the uncertain parameters, but they were adjusted to give a good match to the total number of metal-poor GCs observed in the real Milky Way.

Our adopted value ($F_{\rm ion} = 210$) of the ionization efficiency corresponds to the suppression of GC formation after a redshift of $z_{\rm ion} = 13$. (Even if we allow for a possible factor of 2 uncertainty in $F_{\rm ion}$, this only gives a range of $z_{\rm ion} = 10$–15.) This redshift is significantly higher than the estimates of the reionization redshift of the Universe derived from quasi-stellar object studies ($z_{\rm reion} = 6.4$), but if GCs form high-mass stars first, then the local *intra*-cluster medium is going to be far more ionized than the rest of the Universe.

This model, whereby GC formation is truncated when the clusters themselves reionize the remaining gas in the protogalaxy, has one important feature: it naturally predicts that the number of metal-poor GCs is proportional to the baryonic mass of the galaxy. For a constant mass-to-light ratio, this is directly equivalent to saying that galaxies of this type will all have the same specific frequency of GCs, S_N. The prediction of proportionality is robust even with the uncertainty in the ionizing efficiency calculation; if this calculation becomes more precise, we will also be able to predict the absolute values of specific frequency.

Given that our model has involved some adjustment of one parameter to match one observable (the total number of GCs formed), its success can be demonstrated by testing it against other observations. In Section 3, we showed that the model successfully reproduces both the radial distributions and the ages of the metal-poor GCs. The agreement with these two independent measurements gives us a high degree of confidence in our model.

An important concern for both the metal-poor and the metal-rich models is that the results should not be biased by the resolution of the particular simulation used. We can test this in a very straightforward manner for the current models by repeating the models with a lower resolution simulation: if the same results are obtained, this demonstrates that our models are not affected by mass resolution. Our main analysis uses the AqA2 simulation (mass resolution of $1.370 \times 10^4\,{\rm M}_\odot$); we have repeated both models with the lower resolution AqA3 simulation (mass resolution of $4.911 \times 10^4\,{\rm M}_\odot$). In Fig. 9 we show the result of the comparison by plotting the radial distributions of both metal-poor and metal-rich GCs produced in both simulations. For both models, the agreement is excellent: the total numbers produced agree to within 5 per cent and a KS test shows that they are drawn from the same distribution. This agreement shows that the results are not biased by the resolution of the simulations used. Note that complete agreement is not expected for a variety of reasons: the extra substructure will cause haloes to form at slightly different times and the trajectories of the most bound particles will also be altered. (The lower resolution AqA3 model of metal-rich GCs extends to larger radii in Fig. 9 than the corresponding AqA2 objects only because of two haloes at large radii that are just below the mass limit in AqA2, but have slightly higher masses in the low-resolution simulation.)

In our model of the metal-poor GCs, we use the most bound particle (at the time of formation) of the dark matter halo hosting each GC to trace the final positions of GCs whose haloes have merged with the central galaxy halo. Note that we do not spatially resolve the internal structure of these first haloes. However, we would expect the GC to form at the dynamical centre of the halo and so we associate it with the most bound particle in the halo.

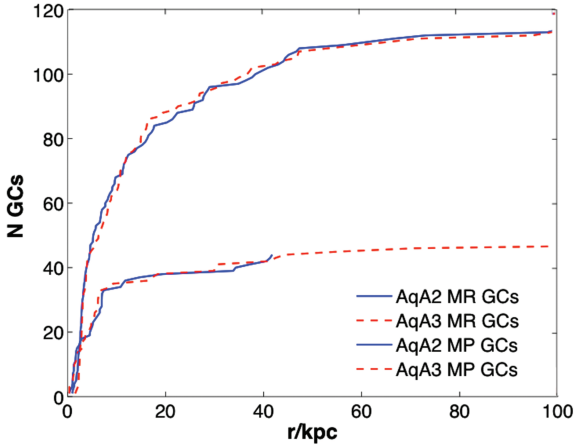

Figure 9. Tests of the effect of the simulation mass resolution on our GC formation models. We plot the radial distributions of both metal-poor and metal-rich GCs produced using both the original simulation (AqA2, $1.370 \times 10^4\,{\rm M}_\odot$, solid lines) and the lower resolution AqA3 simulation ($4.911 \times 10^4\,{\rm M}_\odot$, dashed lines). The metal-poor GCs are shown by the upper two curves and the smaller metal-rich GCs by the lower two curves. In both cases the results at the two resolutions are entirely consistent, showing that our results are not affected by the resolution of the simulations.

In this work, we do not specifically model any processes that could destroy the GCs after their formation. Such processes could potentially remove GCs from our final predicted distributions. Possible processes which may disrupt our GCs are dynamical friction, bulge and disc shocking and tidal disruption. The time-scale for dynamical friction (Chandrasekhar 1943) is inversely proportional to mass, so the GCs will be more affected by this process than the dark matter particles (which are of the order of 100 times less massive). For GCs of mass a few times $10^5\,{\rm M}_\odot$ at radii of 10 kpc the dynamical friction time-scale is 10^{12} yr, so this is unlikely to affect our results. Gnedin, Lee & Ostriker (1999) showed that both disc and bulge shocks can shorten the GC destruction times from 24 to 18 Gyr. Since these processes act over much longer time-scales than the total age of our GCs, their effect on removing stellar content from the most bound dark matter particle would be minimal. Tidal effects can totally disrupt GCs on time-scales from 10^9 to over 10^{10} yr (Baumgardt & Makino 2003), but the time-scales are very dependent on the initial masses and orbits of the GCs. Tidal disruption may be significant for these GCs on highly radial orbits, but a much more detailed model of the evolution of the cluster candidates would be required to investigate this effect which we defer to future work.

We have also used the model to estimate the final masses of the GCs. This involves a much higher degree of uncertainty as we have to estimate the efficiencies of both cluster formation and its subsequent evolution. We adjusted the star formation efficiency to give mean masses consistent with the Milky Way GCs, but the results then suggest a slightly narrower range of mass than in observed clusters. Interestingly, our results do not provide strong evidence for a power-law distribution in the masses of the metal-poor GCs at formation as has been assumed in some studies of their subsequent evolution (Prieto & Gnedin 2008). In future work, it would be valuable to investigate the evolution of the GCs formed in our model in a similar way.

The approach used above to estimate the GC masses was necessary in part because most of the GCs we analyse do not survive as separate haloes to the present day, but merge with the main halo.

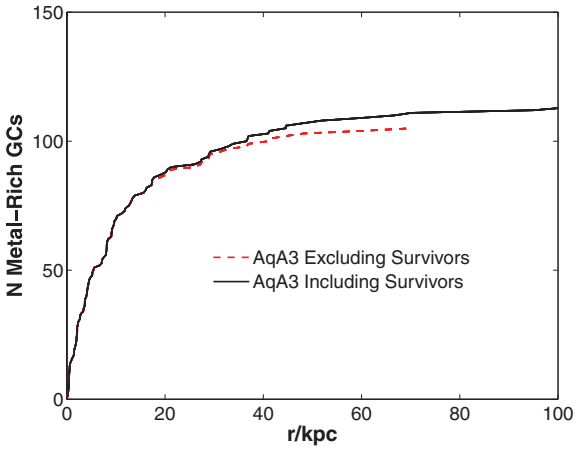

Figure 10. The distribution of metal-poor GC candidates with surviving dark matter haloes. The plot compares the radial distribution of all metal-poor GC candidates with those that have merged (upper solid line) completely with the central halo by redshift $z = 0$. The lower dashed line shows the distribution of metal-poor GCs but excludes those which have not merged with the central halo by $z = 0$. The small gap between the two distributions indicates how few GCs have surviving dark matter haloes this close to the Galaxy.

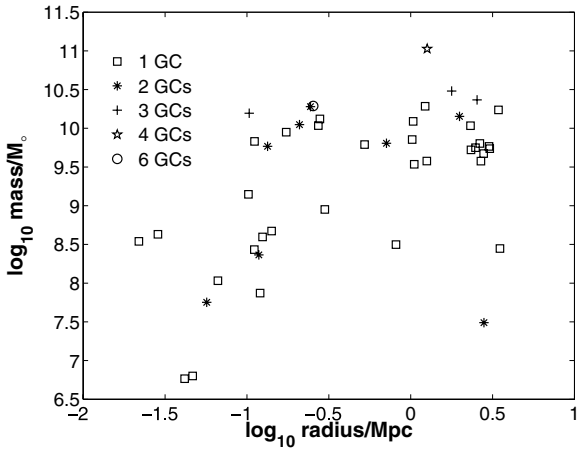

Figure 11. The properties of haloes which have not merged with the central galaxy halo at redshift $z = 0$ and contain metal-poor GC candidates. Each point gives the mass and projected radius from the central galaxy of a dark matter subhalo containing at least one metal-poor GC candidate. The symbols indicate how many GCs each contains (1: squares; 2: asterisks; 3: crosses; 4: stars; 6: circles). The distribution of masses and radii is very similar to that of observed dwarf galaxies in the Local Group.

This is demonstrated by Fig. 10, which compares the total radial distribution at redshift zero of all the metal-poor GCs to those which have merged with the central halo. The gap between the two curves in the figure indicates the small number of GCs still found in surviving haloes; this is a very small fraction, less than 10 per cent within a radius of 100 kpc. The presence of these surviving haloes does suggest that some GCs associated with the Milky Way will have retained some dark matter, but at relatively large radii, these may be associated with dwarf satellite galaxies rather than isolated GCs.

If we now consider all the GCs found in surviving dark matter haloes distinct from the central halo in the full simulation (i.e. at larger distances from the main halo), we can measure their (dark matter) masses and positions as shown in Fig. 11. In this figure, there are 47 distinct haloes containing 68 GCs and the haloes which contain more than one GC are indicated by different symbols. The overall spread of properties is quite similar to that of dwarf galaxies in the Local Group, both in distance and in mass (Mateo 1998). The objects in the figure can be divided into two groups. The smaller haloes ($<2 \times 10^9\,M_\odot$) are nearly all at small radii (<100 kpc) and are single GCs: these presumably correspond to small satellite galaxies of the Milky Way that still retain some dark matter. On the other hand, the more massive haloes ($>2 \times 10^9\,M_\odot$) tend to lie at large radii (>100 kpc) and often contain multiple GCs. These correspond to the larger dwarf galaxies of the Local Group. Georgiev et al. (2009) studied 10 late-type dwarf galaxies between 3 and 6.5 Mpc from the Milky Way and found each of them harbouring significant GC populations, some stretching out to 5 kpc from the dwarf host. We also find a number of these such systems in the 2–3 Mpc range, as shown in Fig. 11. We must note, however, that our metal-poor GC formation model does not necessarily apply to the more distant objects as they would not have experienced the same ionization environment as those forming closer to the main halo.

In a related study of the Aquarius simulations, Gao et al. (2010) have investigated the formation of the very first stars, systems with temperatures around 10^3 K that form at redshifts of $z = 20$ or higher. In this context, they also considered systems formed by line cooling (10^4 K) at later times. These objects are very similar to what we identify as candidate GC formation sites in this paper, although Gao et al. refer to them as 'first galaxies' and focus on a comparison of the surviving objects with observed dwarf galaxies around the Milky Way, obtaining similar results to those we describe here. The primary difference is that we propose that these 'first galaxies' are in fact the primordial metal-poor GCs we observe today.

As we note above, our model for the formation of the metal-rich GCs relies on several assumptions; it is mainly intended to let us determine if any class of model can come close to reproducing the extremely concentrated distribution of these objects observed in the Milky Way. Our merger model is significantly better than any hierarchical model we have considered in reproducing the observed combination of a centrally concentrated distribution and young ages for these objects. The model does produce a few metal-rich GCs at larger radii and younger ages than observed in the Milky Way. However, this could be an accident of the formation history of the halo and so further investigation is required. Furthermore, if the observational data set were incomplete due to obscuration by the bulge then the true distribution would be even more centrally concentrated. This, in turn, would be even harder to reproduce within the hierarchical scenario we have examined. In either case, our metal-rich GC formation model still points to merging as the most likely scenario to produce the bulk of the centrally located GCs we observe today.

6 SUMMARY AND FUTURE WORK

In this study, we have made use of the exquisite resolution of the Aquarius simulations to test plausible metal-poor and metal-rich GC formation models. Here, we summarize our main results and indicate our plans for future work.

6.1 Metal-poor GCs

We adopted a relatively simple formation scenario for metal-poor GCs by identifying all haloes which go above the 10^4 K threshold

required to cool and form stars. We then measured the ionizing contribution from the very first GCs and calculated when the entire Galaxy became ionized. When this occurred, we halted GC formation.

There is some uncertainty in our calculation of the amount of ionization from the first GCs. We have therefore treated this as a free parameter which we have adjusted so that our model produces a similar total number of metal-poor GCs to those observed in the Milky Way. Even though this has been adjusted, we should emphasize that the values chosen are quite reasonable and that changing the value by as much as a factor of 2 will only vary the redshift when GC formation is suppressed over the range of $z_{\rm ion} =$ 10–15. Our adopted value of the ionization contribution (mass of baryons ionized per mass of baryons in the halo forming each GC) is $F_{\rm ion} = 210$. This results in the galaxy being ionized by a redshift of $z_{\rm ion} = 13$ when 173 metal-poor GCs have formed.

We have tested this model for the effects of numerical resolution by repeating the analysis for a lower resolution simulation. We obtained almost identical results between the two resolution runs, indicating that the model is not biased by the simulation resolution.

Having fixed the number of GCs, we then find that the model successfully predicts two independent properties of the metal-poor GCs: their spatial distribution and formation ages of the GCs. The radial distribution of the model GCs shown in Fig. 5 is a very good match to that of the observed Milky Way population. We obtain mean ages of 13.3 Gyr, consistent with observations by Marín-Franch et al. (2009). The agreement of our model with these two independent observations provides strong support for our approach.

We can also estimate the final masses of the GCs if we introduce a second variable parameter, the star formation efficiency in the protoclusters. We have adjusted this (again within reasonable values) to match the observed masses of Galactic metal-poor GCs. Although the mean mass has been set, we note that we predict a narrower *range* of mass than observed.

6.2 Metal-rich GCs

Our approach to the formation of metal-rich GCs is much more qualitative as the process is much more dependent on gas processes that are not directly described in the current simulations. Our aim was to find classes of model that could reproduce distributions like those of Galactic metal-rich GCs which are much more centrally concentrated than the metal-poor GCs. This distribution cannot be produced by hierarchical processes because the metal-rich GCs are younger than the metal-poor GCs; in hierarchical processes, it is always the oldest objects that are most centrally concentrated.

We tested two formation mechanisms: cluster formation triggered in the gas disc of the central halo by large *merging* events and the stripping of infalling haloes (presumed to contain GCs) as they merge with the central halo. We rejected the stripping model because it produces a spatial distribution of GCs in the present day that is far too extended (see Fig. 7).

The only model that produced a sufficiently central distribution was the merger model. In this model, we consider that GCs form when galactic haloes of mass larger than $8 \times 10^8\,{\rm M}_\odot$ merge with a larger halo. We then assume that the GC formation takes place in the central gas disc at a radius estimated as 0.1 times the dark matter half-mass radius. Although there are quite a few assumptions in this model, this model produces the correct distribution. The model also predicts a large spread of ages (3–13 Gyr) that is mostly consistent with the observed Galactic age estimates of Marín-Franch et al. (2009).

As with the metal-poor GCs, we find that this model is not biased by the simulation resolution; when we apply the model to the lower resolution simulation, there is no observable change in the radial distributions within 100 kpc of the central halo.

6.3 Future work

There are a number of avenues for future work. Similar analysis could be carried out on the remaining five Aquarius haloes. They have slightly different central halo masses and spatial resolutions, so they will allow us to test the same formation mechanisms across subtly different evolutionary environments. We have already carried out similar calculations on the AqF Aquarius halo and found comparable results.

The next major step is to introduce semi-analytic modelling. This could give insight into how merger events and halo accretion can alter GC properties. With respect to the metal-rich GCs, the nature of the gas disc during each merger event could be inferred from such models and used to more accurately determine where in the Galaxy these star-forming regions will occur.

Future work will also include GC formation within the Millennium-II (MII) Simulation which, although it has a lower resolution ($m_{\rm p} \sim 6.9 \times 10^6\,{\rm M}_\odot$), can still locate GC formation sites with a minimum of 10 particles per GC. The scale of the MII simulations (box-side length of 100 Mpc h^{-1}) will enable us to correlate GC properties with those of their hosts in a wide range of physical environments.

ACKNOWLEDGMENTS

We wish to thank Bill Harris for many valuable comments about the observational data.

The simulations for the Aquarius project were carried out at the Leibniz Computing Center, Garching, Germany, at the Computing Centre of the Max-Planck Society in Garching, at the Institute for Computational Cosmology in Durham and on the 'STELLA' supercomputer of the LOFAR experiment at the University of Groningen.

This work was supported by travel funding from the Australian Research Council (grant LX0775963). PAT was partially supported by an STFC rolling grant. BFG would like to acknowledge the support provided by the University of Queensland via a University of Queensland Postgraduate Scholarship.

REFERENCES

Ashman K. M., Zepf S. E., 1992, ApJ, 384, 50
Ashman K., Zepf S., 1998, Globular Cluster Systems. Cambridge Univ. Press, Cambridge
Baumgardt H., Kroupa P., 2007, MNRAS, 380, 1589
Baumgardt H., Makino J., 2003, MNRAS, 340, 227
Beasley M. A., Baugh C. M., Forbes D. A., Sharples R. M., Frenk C. S., 2002, MNRAS, 333, 383
Bekki K., 2005, ApJ, 626, 93
Bekki K., Yahagi H., Nagashima M., Forbes D. A., 2008, MNRAS, 387, 1131
Bianchi S., Cristiani S., Kim T.-S., 2001, A&AS, 376, 1
Brodie J. P., Strader J., 2006, ARA&A, 44, 193
Chandrasekhar S., 1943, ApJ, 97, 255
De Angeli F., Piotto G., Cassisi S., Busso G., Recio-Blanco A., Salaris M., Aparicio A., Rosenberg A., 2005, AJ, 130, 116
Eggen O. J., Lynden-Bell D., Sandage A. R., 1962, ApJ, 136, 748
Forbes D. A., Brodie J. P., Grillmair C. J., 1997, AJ, 113, 1652

Gao L., Theuns T., Frenk C. S., Jenkins A., Helly J. C., Navarro J., Springel V., White S. D. M., 2010, MNRAS, in press (arXiv:0909.1593) (doi:10.1111/j.1365-2966.2009.16225.x)
Georgiev I. Y., Hilker M., Puzia T. H., Goudfrooij P., Baumgardt H., 2009, MNRAS, 396, 1075
Gnedin N. Y., Hamilton A. J. S., 2002, MNRAS, 334, 107
Gnedin O. Y., Lee H. M., Ostriker J. P., 1999, ApJ, 522, 935
Harris W. E., 1996, AJ, 112, 1487
Holtzman J. A. et al., 1992, AJ, 103, 691
Kravstov A. V., Gnedin O. Y., 2005, ApJ, 623, 650
Kruijssen J. M. D., 2008, A&AS, 486, L21
Leitherer C. et al., 1999, ApJS, 123, 3
Madau P., Shull J. M., 1996, ApJ, 457, 551
Maraston C., 2005, MNRAS, 362, 799
Marín-Franch A. et al., 2009, ApJ, 694, 1498
Mateo M. L., 1998, ARA&A, 36, 435
Moore B., Diemand J., Madau P., Zemp M., Stadel J., 2006, MNRAS, 368, 563
Nishi R., 2002, Progress Theor. Phys. Suppl., 147, 1
Ostriker J. P., Steinhardt P. J., 1995, Nat, 377, 600
Peebles P. J. E., 1984, Sci, 224, 1385
Power C., Wynn G. A., Combet C., Wilkinson M. I., 2009, MNRAS, 395, 1146
Prieto J. L., Gnedin O. Y., 2008, ApJ, 689, 919
Ricotti M., 2002, MNRAS, 336, L33
Salaris M., Weiss A., 2002, A&AS, 388, 492
Schweizer F., 1987, in Faber S. M., ed., Nearly Normal Galaxies: From the Planck Time to the Present. Springer, New York, p. 18
Searle L., Zinn R., 1978, ApJ, 225, 357
Sokasian A., Yoshida N., Abel T., Hernquist L., Springel V., 2004, MNRAS, 350, 47
Springel V., White S. D. M., Tormen G., Kauffmann G., 2001, MNRAS, 328, 726
Springel V. et al., 2005, Nat, 435, 629
Springel V. et al., 2008, MNRAS, 391, 1685 (S08)
Srbinovsky J., Wyithe S., 2006, preprint (astro-ph/0610306)
Toomre A., Toomre J., 1972, ApJ, 178, 623
Tumlinson J., Venkatesan A., Shull J. M., 2004, ApJ, 612, 602
Weidner C., Kroupa P., Nürnberger D. E. A., Sterzik M. F., 2007, MNRAS, 376, 1879
West M. J., Côté P., Marzke R. O., Jordan A., 2004, Nat, 427, 31
Whitmore B. C., Schweizer F., 1995, AJ, 109, 960
Zepf S. E., 2009, The Formation Histories of Metal-Rich and Metal-Poor Globular Clusters. Springer, Berlin, p. 339

APPENDIX A

Here we estimate $\bar{q}$, the mean number of ionizing photons per baryon, averaging over a Salpeter IMF. The calculation is easily extended to other mass functions that can be approximated as a power law above $10\,\mathrm{M}_\odot$.

The Salpeter IMF is

$$\mathrm{d}n = \frac{(\alpha-2)\,M}{m_0}\left(\frac{m}{m_0}\right)^{-\alpha}\frac{\mathrm{d}m}{m_0}, \qquad m \geq m_0, \tag{A1}$$

where $\mathrm{d}n$ is the number of stars in the mass interval $m \mapsto m + \mathrm{d}m$, M is the total mass of stars, and $\alpha = 2.35$ and $m_0 = 0.1\,\mathrm{M}_\odot$ are parameters describing the slope and lower mass cut of the population, respectively.

The number of ionizing photons per baryon as a function of stellar mass for a typical Population II metallicity of 0.001, derived using the STARBURST99 code of Leitherer et al. (1999), is given in fig. 2 of Tumlinson et al. (2004). We approximate this a sequence of piecewise, linear fits in $\lambda = \log_{10}(m/\mathrm{M}_\odot)$:

$$q \approx \begin{cases} 30\,000\,(\lambda - 1.00), & 1.00 < \lambda < 1.18 \\ 108\,000\,(\lambda - 1.13), & 1.18 < \lambda < 1.72 \\ 20\,000\,(\lambda + 1.47), & 1.72 < \lambda < 2.10. \end{cases} \tag{A2}$$

Tumlinson et al. (2004) do not give the value of q for masses above $120\,\mathrm{M}_\odot$; there are a few stars of this mass and so their contribution to $\bar{q}$ is relatively small: we simply take q to be constant in this regime.

Within each piecewise interval, the contribution to $\bar{q}$ is

$$\bar{q} = \int_{m_1}^{m_2} q\,(\alpha-2)\left(\frac{m}{m_0}\right)^{1-\alpha}\frac{\mathrm{d}m}{m_0} \tag{A3}$$

$$= \int_{\mu_1}^{\mu_2} k_q\,(\alpha-2)\log_{10}(\mu/\mu_k)\,\mu^{1-\alpha}\mathrm{d}\mu, \tag{A4}$$

where $\mu = m/m_0$ and k_q and μ_k are appropriate constants taken from equation (A2). This integrates to give

$$\bar{q} = k_q\left[\left(\log_{10}(\mu/\mu_k) + \log_{10} e/(\alpha-2)\right)\mu^{2-\alpha}\right]_{\mu_2}^{\mu_1}. \tag{A5}$$

This expression can be simplified by noting that, when summing these expressions over the whole mass range, the first term in the square brackets vanishes whenever q is a continuous function.

Putting in values appropriate to a Salpeter IMF gives $\bar{q} \approx 10\,000$.

This paper has been typeset from a TEX/LATEX file prepared by the author.